Supporting information for:

Roll-To-Roll Deposition of Semiconducting 2D Nanoflake Films of Transition Metal Dichalcogenides for Optoelectronic Applications

Rebekah A. Wells,[1] Hannah Johnson,[1,2] Charles Lhermite,[1] Sachin Kinge,[2] Kevin Sivula[1]*

1. Laboratory for Molecular Engineering of Optoelectronic Nanomaterials (LIMNO), Institute of Chemical Sciences and Engineering, École Polytechnique Fédérale de Lausanne, 1015 Lausanne, Switzerland.

2. Advanced Materials Research, Toyota Motor Europe, B-1930 Zaventem, Belgium.

*kevin.sivula@epfl.ch

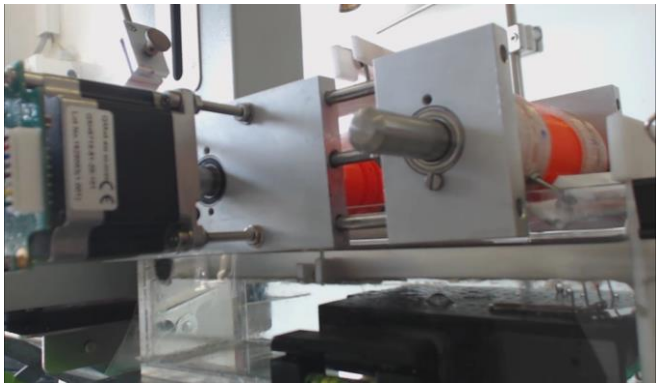

Movie S1 (separate download): Video recording of MoS_2 film formation in roll-to-roll (R2R) apparatus. TMD dispersion is injected via four needles in the water layer and a film forms at the water-heptane interface. Then, this film is compressed by the rotating paddle and moved towards the substrate roll located in the bath at the interface. The film is then transferred onto the flexible substrate as it moves up and out of the bath.

Movie S2 (separate download): Additional video recording of MoS_2 nanoflake film deposition onto a flexible plastic substrate.

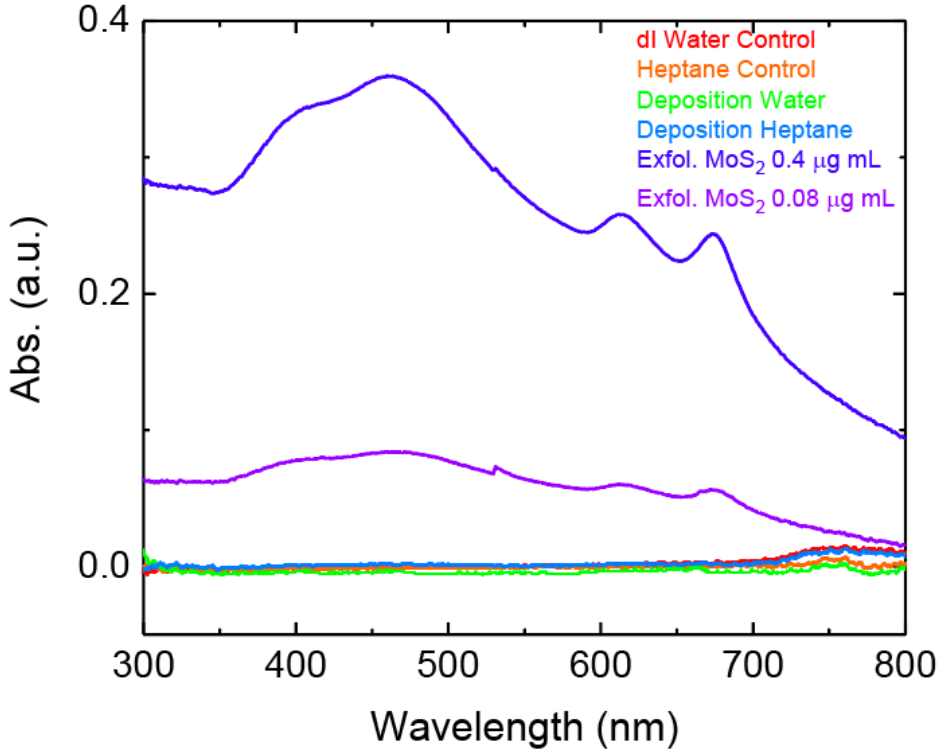

Figure S1: Ultraviolet-visible spectroscopy for the R2R solvent system. The red and orange curves show controls for water and heptane, respectively. The blue and green curves show samples for heptane and water, respectively, which were taken after several consecutive film depositions had been performed in the same solvent bath. The violet and purple curves give the absorption spectra for trace amounts of MoS_2 dispersed in the 1:10 by volume tert-butanol/1-butanol mixture. Importantly, no trace of MoS_2 is observed in either of the solvents after the film deposition.

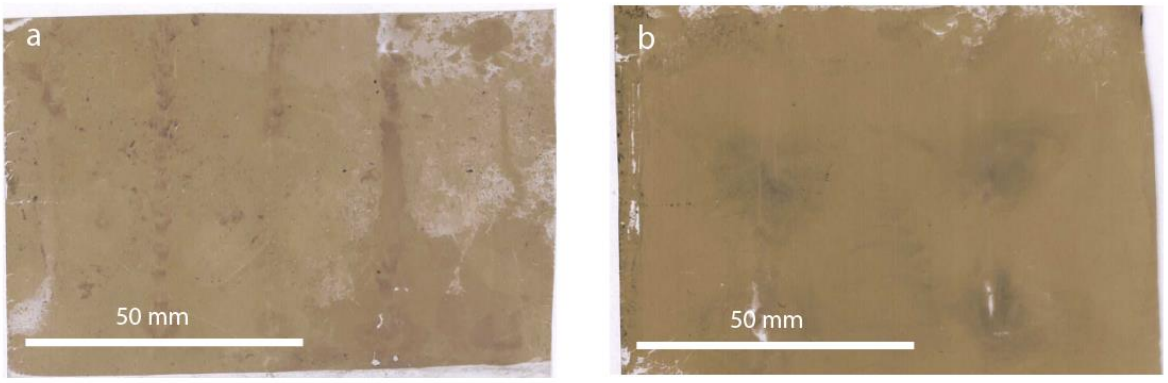

Figure S2: (a) MoS_2 deposited on flexible PET substrate in semi-continuous mode using a needle array containing 16 needles and (b) MoS_2 deposited on flexible PET substrate in semi-continuous mode using a needle array containing four injection sites. Despite injecting over the same area, the film shown in image b is more uniform than the film shown in image a. Though some dark areas can still be observed for the four injection sites, they are less apparent and produce an overall more uniform film than when four times as many needles are present.

Dispersion volume injection rate (mL min^{-1})	**Dispersion injection duration (s)**	**Final Nanoflake loading per substrate area (mg m^{-2})**	**Nanoflake loading rate per substrate area (mg s^{-1} m^{-2})**
2	13.5	45	3.3
9	2.53	38	15
15	1.88	47	25

Table S1: Summary of parameters used in the semi-continuous deposition injection rate study. A 100 mm by 100 mm liquid-liquid interface was used. Injection rate was controlled via syringe pumps, which could then be translated into flake loading and finally loading rate. For each loading rate similar flake loading per area was observed. Therefore, the large difference in film formation observed in Figure 2a-c is solely a result of the nanoflake loading rate.

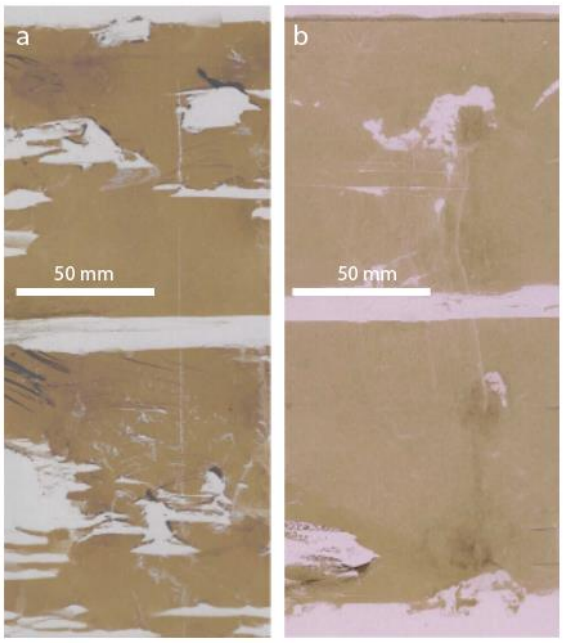

Figure S3: (a) MoS_2 deposited on as-received ITO-coated PET (solaronix) and (b) UV-treated ITO-coated PET. It is clear that the MoS_2 nanoflakes are better able to adhere to the treated substrate resulting in a better film transfer and a uniform final product.

Figure S4: Three MoS_2 films deposited in continuous mode on flexible plastic substrate demonstrate that our R2R system can consistently produce large-area thin-films of semiconducting nanoflakes of similar quality.

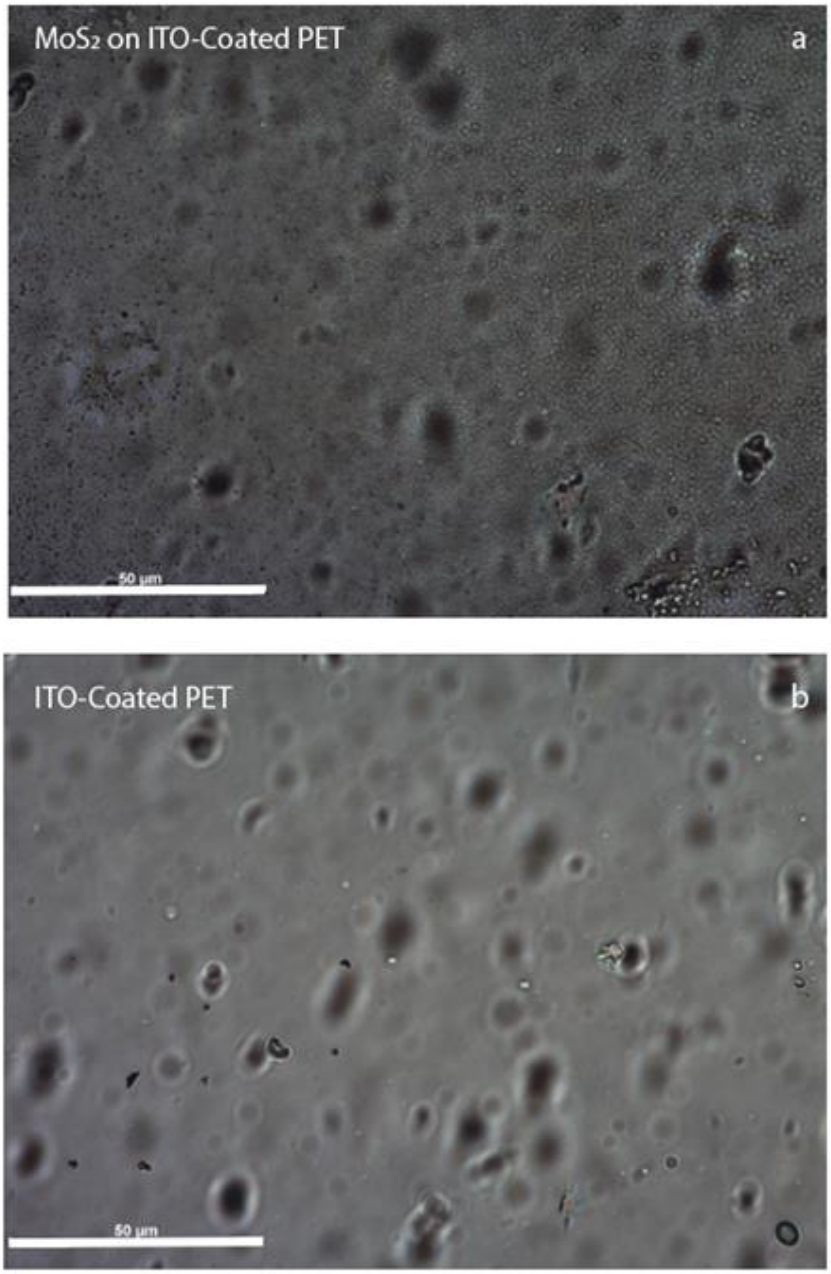

Figure S5: (a) Optical microscopy of a R2R MoS_2 film on ITO-coated PET. (b) Optical microscopy of cleaned ITO-coated PET. It can be seen that the ITO-coated PET substrate is full of defects and deformities, rather than the TMD films.

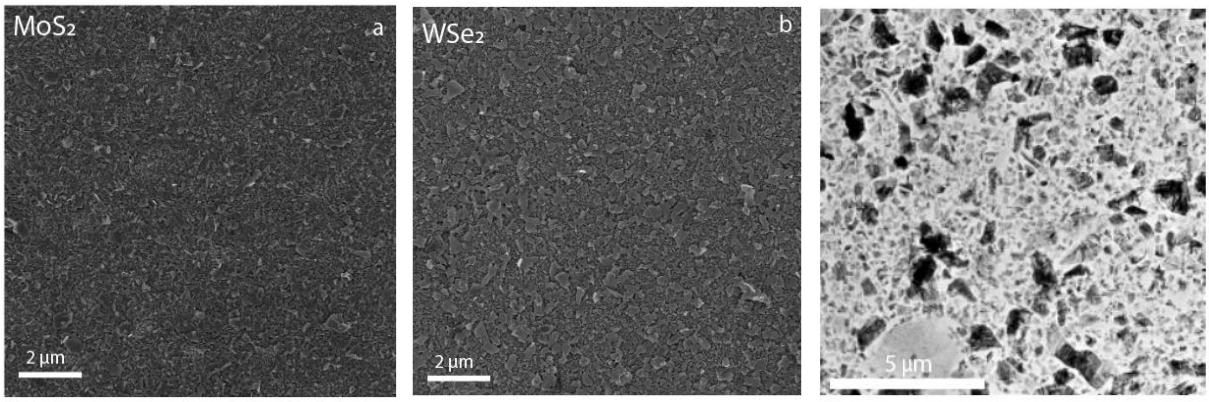

Figure S6: Scanning electron microscopy of batch films deposited on FTO-coated glass, MoS_2 (a) and WSe_2 (b). Transmission electron microscopy of a batch film of MoS_2 on a SiN grid (c), where dark represent thicker flakes, grey represents thinner flakes, and white represents unfilled space. Film coverage is estimated at 80%. Film morphology shows good flake-to-flake alignment and, importantly, no large aggregates. We observe no notable difference between film morphology of the batch and R2R films.

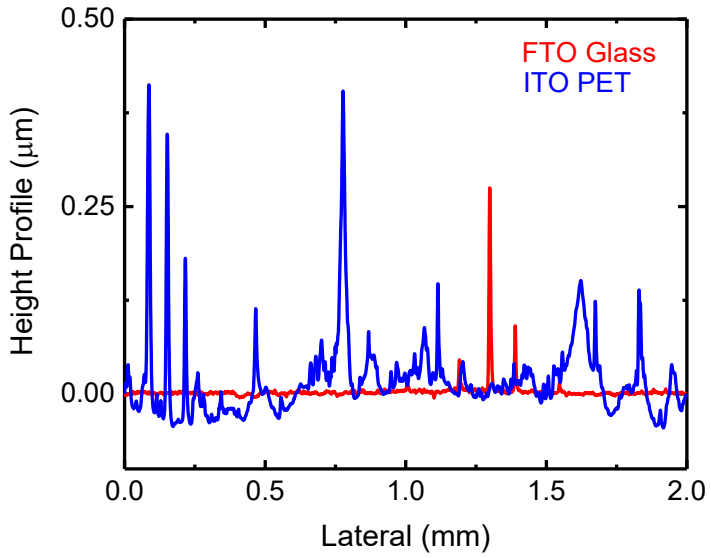

Figure S7: Profilometry of blank substrates shows that the conductive, flexible ITO-coated PET substrate is significantly more rough than the conductive, rigid FTO-coated glass substrate. This contributes to the lowered performance of the MoS_2 films coated on the ITO-coated PET substrates compared to those deposited on FTO-coated glass substrates.

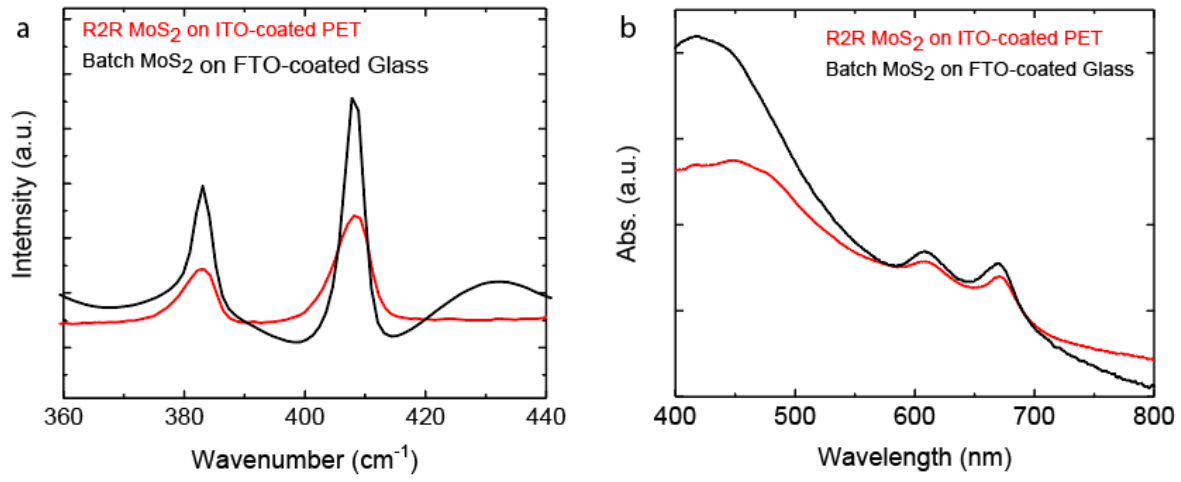

Figure S8: (a) Raman spectroscopy for a R2R (red) and batch (black) film shows the expected MoS_2 vibration modes at 383 cm^{-1} and 408 cm^{-1} for both deposition methods. (b) UV-Vis spectroscopy for a R2R (red) and batch (black) film gives the expected exciton peaks at 610 nm and 670 nm for both films as well as similar absorbance around these values. No miscellaneous solvent peaks, organic residue, or other impurities are observed.

Table S2: Sheet-resistivity as measured by a four-point probe. We note that the manufacturer, Solaronix, lists the sheet resistivity of the ITO-coated PET as 18 ohm/sq.

Substrate	FTO-Coated Glass	ITO-Coated PET
Sheet Resistivity (ohm/sq)	16	30

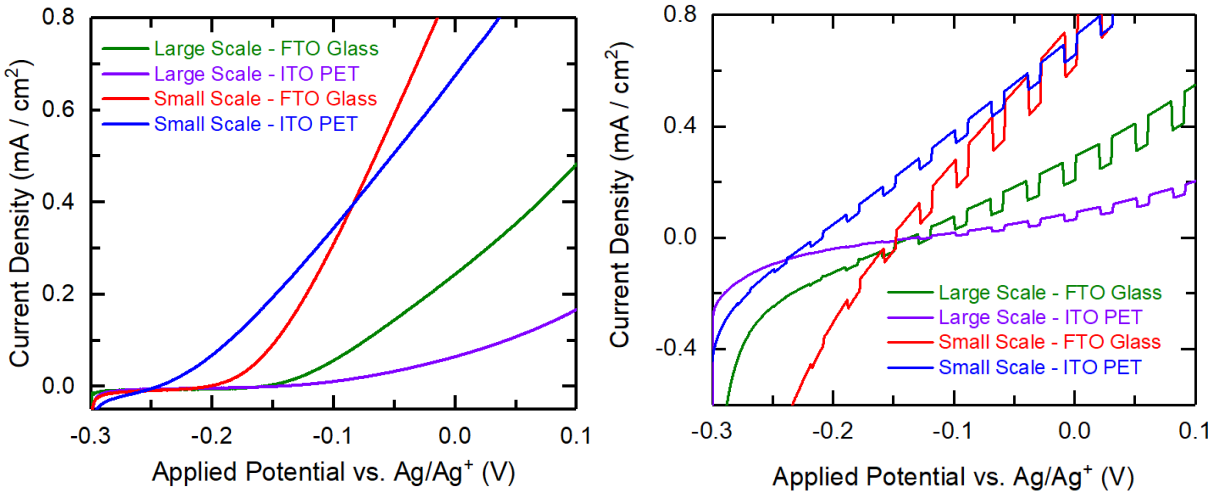

Figure S9: Current-voltage character for R2R and batch films under dark conditions (left) and under intermittent 1-sun illumination (vs. Ag/Ag^+ in 50 mM TBAP 25 mM LiI in MeCN).

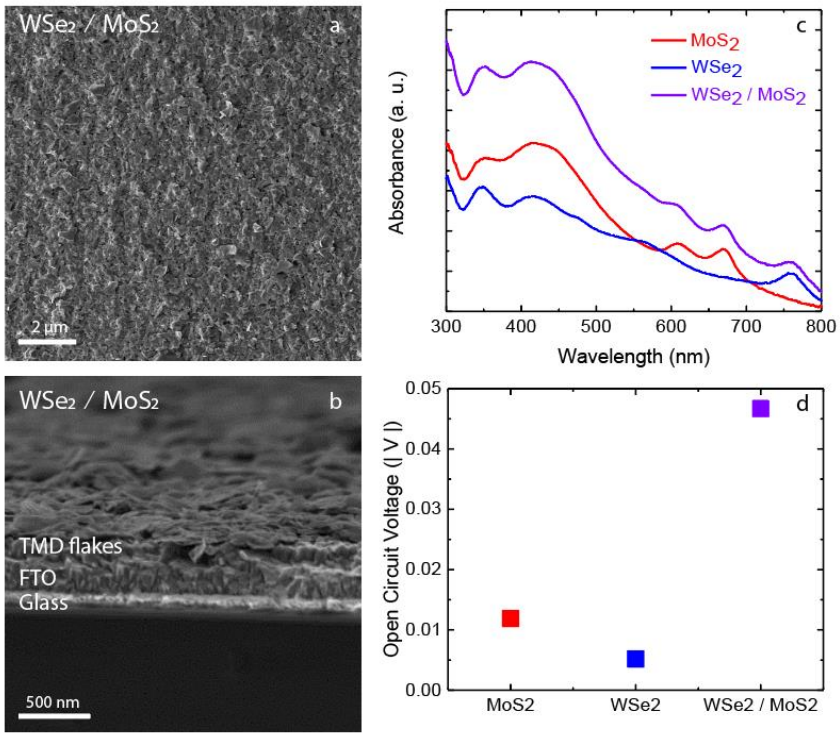

Figure S10: (a) Scanning electron microscopy top view and (b) cross-section view of a batch WSe_2/MoS_2 heterojunction deposited on FTO-coated glass. (c) UV-Vis spectroscopy of the individual films and heterojunction film. (d) Open circuit photopotential of the individual films and the Van der Waals heterojunction in sacrificial conditions (MoS_2: 25 mM LiI and 50mM TBAP in acetonitrile; WSe_2 and WSe_2/MoS_2 : 100 mM NBu_4PF_6 and saturated chloranil in acetonitrile). As in the individual TMD films, SEM images continue to show good flake-to-flake alignment and parallel flake-to-substrate alignment for the heterojunction film. UV-Vis spectroscopy shows that the expected exciton peaks are present for the individual MoS_2 (610 nm and 670 nm) and WSe_2 (760 nm) films as well as in the heterojunction film. As expected, the light absorbance of the heterojunction film is twice that of either of the single films. Open circuit potential for the heterojunction film, however, is not merely additive, but is fundamentally improved. Interfacing these materials allows for electrons and holes to be more efficiently separated in the two materials and for more holes to be stored in the WSe_2, leading to the greatly improved photovoltage seen here.

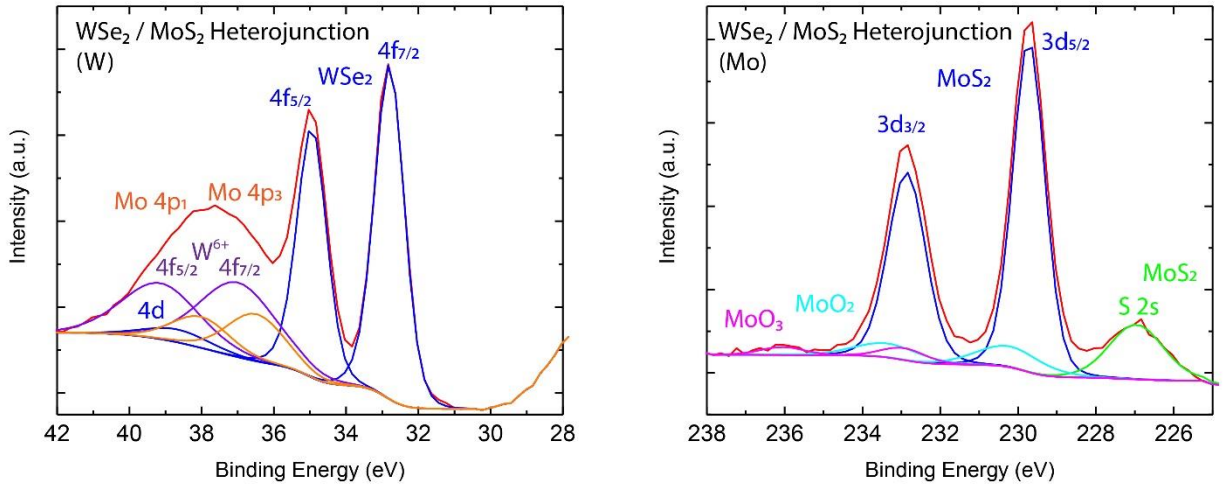

Figure S11: X-ray photoelectron spectroscopy for a batch processed WSe_2 / MoS_2 heterojunction film confirms both material's presence within the same spot. Notably, sputtering was not needed to detect WSe_2 as the MoS_2 layer is extremely thin.

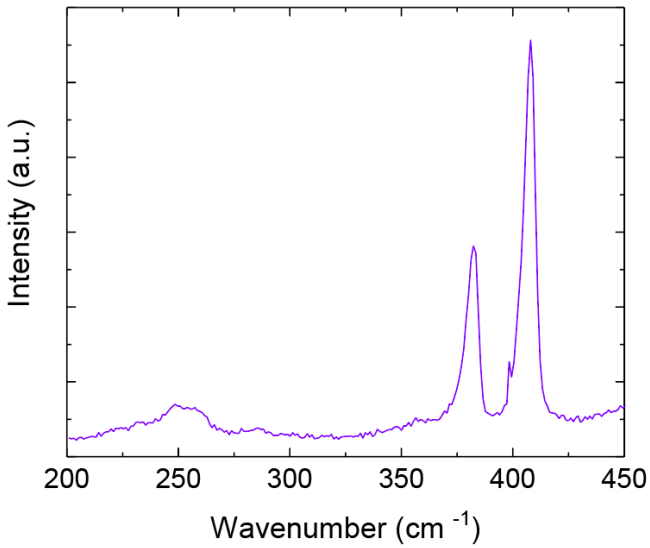

Figure S12: Raman spectroscopy for the R2R heterojunction film presents the expected vibrational modes for MoS_2 (383 cm^{-1} and 408 cm^{-1}) and WSe_2 (250 cm^{-1}) as well as confirms that no miscellaneous peaks are present due to residual solvents, organic residue, or other impurities.

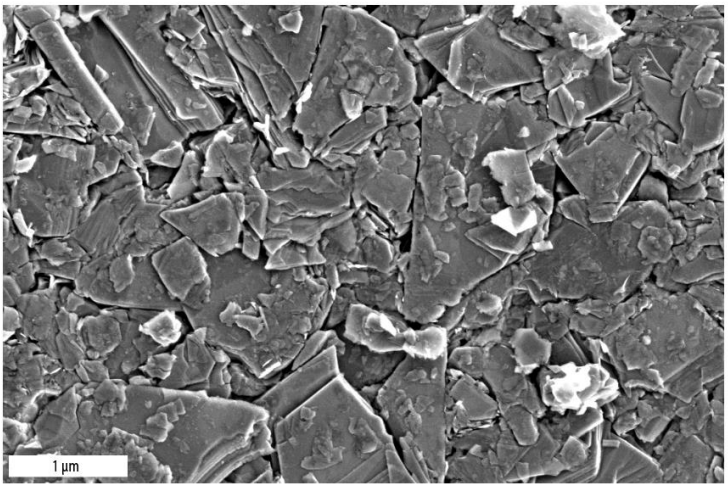

Figure S13: Scanning electron microscopy shows the starting MoS_2 material before exfoliation. The powder, acquired from Alfar Aesar, spans a broad range of sizes and thicknesses. This is in stark contrast to both our batch and R2R films, which were made of dispersions of size-selected flakes. The consistency of the size selection is achieved by keeping centrifugal settings constant for all dispersions.

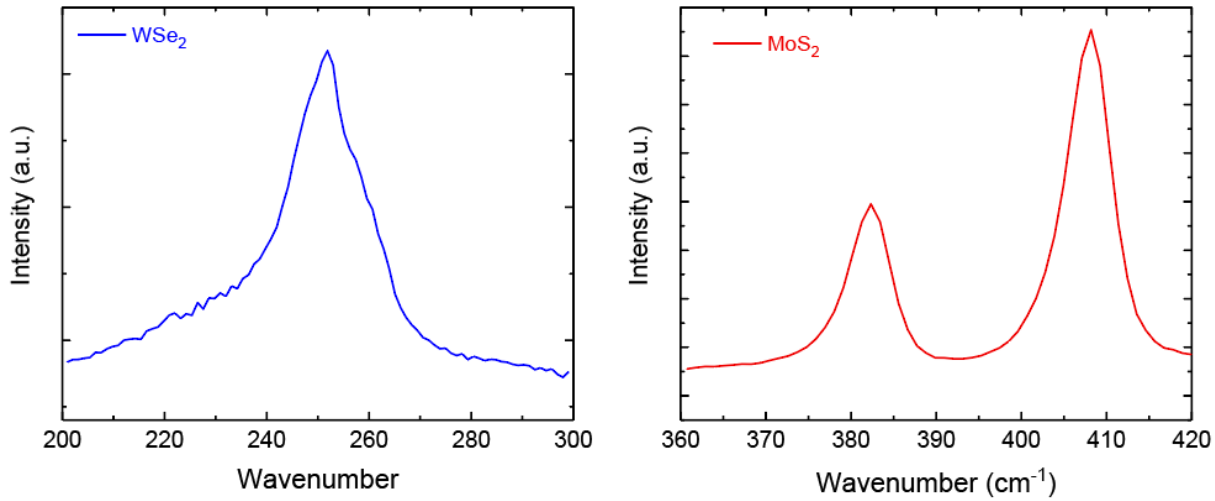

Figure S14: Raman spectroscopy of a drop-casted film of the MoS_2 and WSe_2 dispersions after exfoliation, before injection into the roll-to-roll system. The left figure shows the expected vibration mode for WSe_2 at 250 cm^{-1}, while the right figure shows the expected MoS_2 peaks at 383 cm^{-1} and 408 cm^{-1}. These graphs show that the exfoliated material is pristine before injection into the film deposition system and undergoes no changes during the film deposition process.

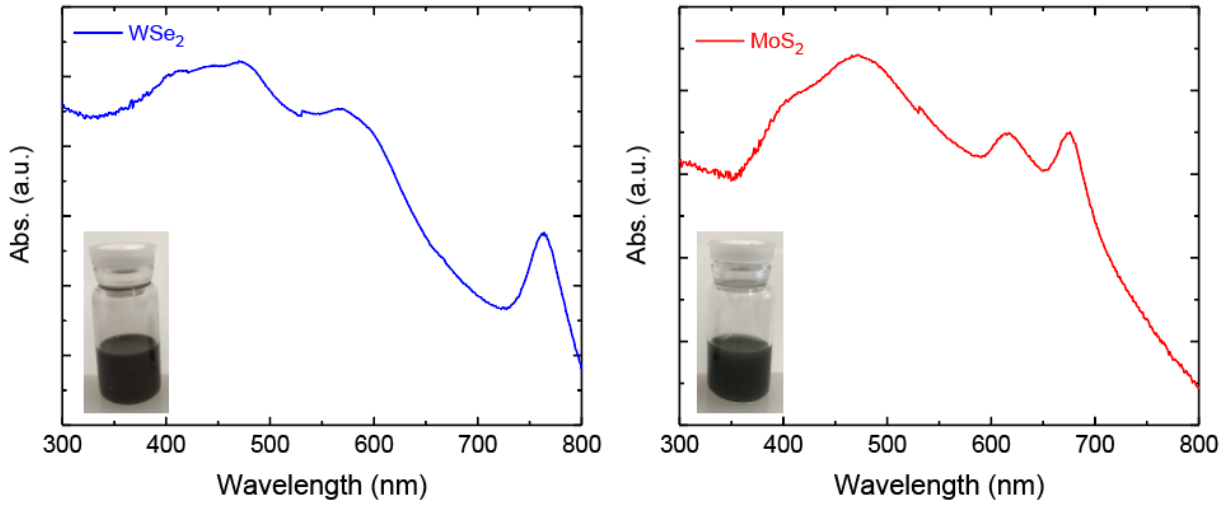

Figure S15: UV-Vis spectroscopy of the MoS_2 and WSe_2 dispersions after exfoliation, before injection into the roll-to-roll system. The left figure gives the expected excitonic peak for WSe_2 at 760 nm and the right figure gives the expected peaks for MoS_2 at 610 nm and 670 nm. These spectra serve as further proof that the nanoflakes within these dispersions display the same properties before and after film deposition, undergoing no changes. Insets: photographs of the 1 mg/mL nanoflake dispersions for each material.